



Contents lists available at ScienceDirect

# Journal of Quantitative Spectroscopy & Radiative Transfer

journal homepage: [www.elsevier.com/locate/jqsrt](http://www.elsevier.com/locate/jqsrt)

## The case for a modern multiwavelength, polarization-sensitive LIDAR in orbit around Mars



Adrian J. Brown<sup>a,\*</sup>, Timothy I. Michaels<sup>a</sup>, Shane Byrne<sup>b</sup>, Wenbo Sun<sup>c</sup>,  
Timothy N. Titus<sup>d</sup>, Anthony Colaprete<sup>e</sup>, Michael J. Wolff<sup>f</sup>, Gorden Videen<sup>f</sup>,  
Christian J. Grund<sup>g</sup>

<sup>a</sup> SETI Institute, 189 Bernardo Ave., Mountain View, CA 94043, USA

<sup>b</sup> Lunar and Planetary Laboratory, 1629 E. University Blvd., Tucson, AZ 85721-0092, USA

<sup>c</sup> Science Systems and Applications, Inc., USA

<sup>d</sup> U.S. Geological Survey, Astrogeology Science Center, Flagstaff, AZ 86001, USA

<sup>e</sup> Space Science Division, NASA Ames Research Center, USA

<sup>f</sup> Space Science Institute, 4750 Walnut St., Suite 205, Boulder, CO 80301, USA

<sup>g</sup> Lightworks, LLC, Boulder, CO 80301, USA

### ARTICLE INFO

#### Article history:

Received 30 May 2014

Received in revised form

28 August 2014

Accepted 28 October 2014

Available online 7 November 2014

#### Keywords:

Mars

LIDAR

Polarization

Müller matrix

Symmetry

Light scattering

### ABSTRACT

We present the scientific case to build a multiple-wavelength, active, near-infrared (NIR) instrument to measure the reflected intensity and polarization characteristics of back-scattered radiation from planetary surfaces and atmospheres. We focus on the ability of such an instrument to enhance, potentially revolutionize, our understanding of climate, volatiles and astrobiological potential of modern-day Mars.

Such an instrument will address the following three major science themes, which we address in this paper:

**Science Theme 1. Surface.** This would include global, night and day mapping of H<sub>2</sub>O and CO<sub>2</sub> surface ice properties.

**Science Theme 2. Ice Clouds.** This would include unambiguous discrimination and seasonal mapping of CO<sub>2</sub> and H<sub>2</sub>O ice clouds.

**Science Theme 3. Dust Aerosols.** This theme would include multiwavelength polarization measurements to infer dust grain shapes and size distributions.

© 2014 Elsevier Ltd. All rights reserved.

### 1. Introduction

Our present understanding of the sublimation of surface H<sub>2</sub>O and CO<sub>2</sub> ices and related atmospheric changes on Mars is the result of recent polewide and seasonal studies of springtime recession using the *CRISM* [1], *Mars Climate Sounder* [2] and *MARCI* [3] instruments on MRO, the *OMEGA* instrument on Mars Express [4,5], the *THEMIS* instrument on Mars Odyssey [6] and the *TES* instrument on Mars Global

Surveyor [7]. These investigations have steadily advanced our understanding of major polar processes. However, the confirmed observations of the spatially localized springtime recession phenomena such as geysers (gas/dust jets) [8] and asymmetric retraction of the seasonal cap [9] lead us to ask the key scientific question – what role does spatially localized and temporally intermittent deposition of ices and dust during fall and winter play in the annual CO<sub>2</sub> and H<sub>2</sub>O cycles which dominate the climate of modern-day Mars?

We discuss herein an instrument concept called “*Atmospheric/Surface Polarization Experiment at Nighttime*” (*ASPEN*) [10] which is designed in response to this first order scientific question regarding Martian climate.

\* Corresponding author. Tel.: +1 650 810 0223.

E-mail address: [abrown@seti.org](mailto:abrown@seti.org) (A.J. Brown).

The *ASPEN* instrument will be a multi-wavelength, altitude-resolved, active near-infrared (NIR) instrument to measure the reflected intensity and polarization characteristics of backscattered radiation from planetary surfaces and atmospheres. The proposed instrument is ideally suited for a mission to Mars to investigate the nature and seasonal abundance of atmospheric dust and icy volatiles, provide insight into surface and cloud/aerosol grain sizes and shapes, evaluate ice and dust particle microphysics and also provide atmospheric column content constituent chemistry during multiple variable overflight local times throughout polar night and day.

Previous instruments have given glimpses of cloud and surface ice activity on Mars, but no previous Martian orbital instrument has been able to simultaneously address the following science questions:

- a) Detect and characterize clouds and condensates up to 100 km above the Martian surface during night and day [11].
- b) Discriminate between H<sub>2</sub>O and CO<sub>2</sub> ice on the surface and aerosols in the atmosphere.
- c) Map the global height of the Martian Planetary Boundary Layer [12] as a function of season [13].
- d) Map cloud structure using lidar backscatter and depolarization.
- e) Map large-grained (up to 30 cm) CO<sub>2</sub> slab ice during the austral polar night [1,14].
- f) Determine whether the H<sub>2</sub>O ice signature in the southern polar trough system is due to cloud [15] or surface ice [16].
- g) Monitor ‘cold spot’ activity during the polar night and determine definitively how these enigmatic features are related to CO<sub>2</sub> clouds, precipitation or surface ice [17,18] or possible low altitude temperature inversions and CO<sub>2</sub> vapor depletion [19].
- h) Monitor night and day gas/dust jet (geyser) activity within the ‘Cryptic Region’ in southern late winter and early spring and determine what amount of solar energy is required for them to be active [8,20].
- i) Uniquely identify cloud types and platelet/grain orientation, in order to confirm the presence and structure of convective CO<sub>2</sub> cloud towers, a potentially critical part of the polar night dynamics and energy partitioning [21].
- j) Provide atmospheric column dust optical depths whenever the instrument is in operation [22,23].
- k) Monitor the spring and summertime retreating polar caps for signs of entrained “sublimation flows” caused by subliming CO<sub>2</sub> ice.
- l) Map the occurrence of unusually thin H<sub>2</sub>O daytime summer polar hoods [24,25].
- m) Address questions of spatial extent (locality and ‘deep transport’) of Martian cloud structure, which is anticipated to be on the order of 1 km width and is crucial to understanding differences between terrestrial and Martian mesospheric atmospheric dynamics [26,27].
- n) Carry out an active circular polarization survey of the selected parts of the surface (e.g. chloride bearing regions [28]) and the ice caps of Mars to determine whether homochiral signatures (a biomarker for terrestrial microbes) exist on the surface [29].

## 2. Instrument concept and background

The Mars Science community has recognized the need for an *ASPEN*-type instrument. The need for active scanning laser sensors that operate over a range of frequencies was acknowledged in the recent Solar System Exploration Roadmap [30] (p. 108). In addition, the Second 2013 Mars Science Orbiter Science Analysis Group (MSO SAG) report stated that a “multibeam lidar” similar to the *LOLA* instrument on Lunar Reconnaissance Orbiter and inheriting many aspects from the *CALIPSO* lidar would “resolve optically dense atmospheric phenomena” and “significantly constrain seasonal mass budgets”. In essence, it was thought to be an ideal instrument for a “2013 MSO mission” [31]. A particular emphasis of this MSO SAG report was the need for focussed Polar investigations. In fact, the SAG designated a suite of specific instruments for “P (Polar) type” observations.

A lidar instrument such as *ASPEN* was also recommended in the report on the 3rd International Workshop on Mars Polar Energy Balance and CO<sub>2</sub> Cycle [32] and has been emphasized further as a future instrument priority in a white paper submitted to the Planetary Sciences Decadal Survey entitled ‘Mars Polar Science for the Next Decade’. Following on after the Mars 2020 rover mission, our targeted mission time frame would be the 2022 launch opportunity and beyond, perhaps as the MICADO Discovery class mission [33].

The scientific impact of such an instrument would be substantial – the Martian climate and its connection to the dynamical environment of the polar nights are unique and poorly understood. Only an active system such as *ASPEN* can adequately investigate the surface and atmospheric characteristics of the Martian polar night.

Fig. 1 shows an artistic rendering of the *ASPEN* lidar system deployed in Mars orbit. The eventual spaceflight instrument will be suited for a mission to Mars to investigate the nature and seasonal abundance of icy volatiles, provide insight into surface and cloud grain sizes

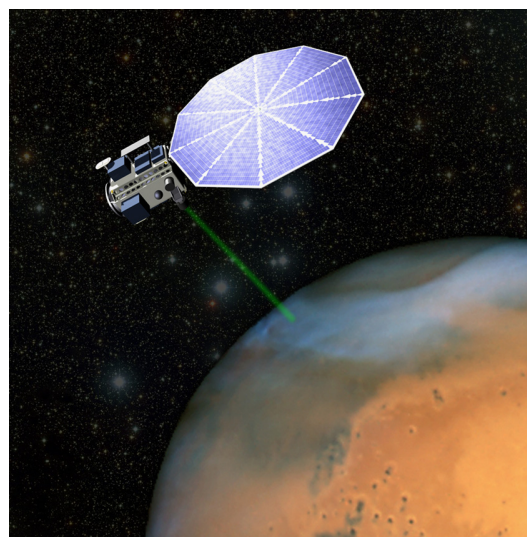


Fig. 1. The *ASPEN* instrument in operation at Mars, probing the north polar hood.

**Table 1**  
Comparison of Lab ASPEN, eventual spaceborne ASPEN, MOLA and CALIOP capabilities. APD=avalanche photon detector.

	Laser source	$\lambda$ ( $\mu\text{m}$ )	Laser (mJ/pulse)	Pulse rate (kHz)	Output pwr (W)	Detector	Mirror diameter/Field of view	Mass (kg)	Power drain (W)
Lab ASPEN	Diode pumped, fiber laser	1.43–1.67	0.04	10	0.4	InGaAs APD	1 in. optics for source and receiver	~30	~50
Space ASPEN	Diode pumped, fiber laser	1.43–1.67	0.04	4.5	0.18	InGaAs APD	80 cm/0.15 mrad	~15	~17
MOLA	Diode pumped, Q-switched Nd:YAG	1.064	48	0.01	0.48	Si-APD	50 cm/0.85 mrad	25.9	34.2
CALIOP	Diode pumped, Q-switched Nd:YAG	0.532, 1.064	110	0.02	2.2	Si-APD	100 cm/0.13 mrad	156	124

and geometries, evaluate cloud/aerosol particle microphysics and potentially also provide atmospheric column constituent chemistry during polar night and day.

*Surface spot size and resolution.* Preliminary laser power calculations of common measurement scenarios for the diode pumped fiber laser ASPEN instrument estimate the surface spot size at  $\sim 25$  m on the surface and a horizontal resolution of  $\sim 275$  m. This is similar to the resolution achieved by the Nd-YAG CALIPSO lidar (Table 1).

*Multiwavelength.* In order to take advantage of the tremendous research and development that has gone into lasers and fiber optic components that operate in the near-IR by the telecommunications industry in recent years, the instrument will operate at wavelengths between 1.43 and 1.67  $\mu\text{m}$ . As we discuss in more detail below, these wavelengths are ideally suited to discriminate  $\text{CO}_2$  and  $\text{H}_2\text{O}$  ices and vapor using the differential absorption lidar (DIAL) technique originally developed for terrestrial remote sensing [34,35].

These particular characteristics of ASPEN are key to generating the type of measurements that will resolve fundamental outstanding questions regarding the Martian climate.

### 2.1. Previous lidar mission – MOLA

The highly successful Mars Orbiting Laser Altimeter (MOLA) instrument on Mars Global Surveyor measured clouds (see Fig. 2) and the height of the seasonal  $\text{CO}_2$  surface ice accumulations [36–38]. However, its use of a single wavelength (1.064  $\mu\text{m}$ ) prevents discrimination between  $\text{H}_2\text{O}$  and  $\text{CO}_2$  clouds using the MOLA dataset, although in combination with TES temperature measurements, causal evidence has been found for polar  $\text{CO}_2$  ice clouds [39]. In addition, MOLA had no ability to determine

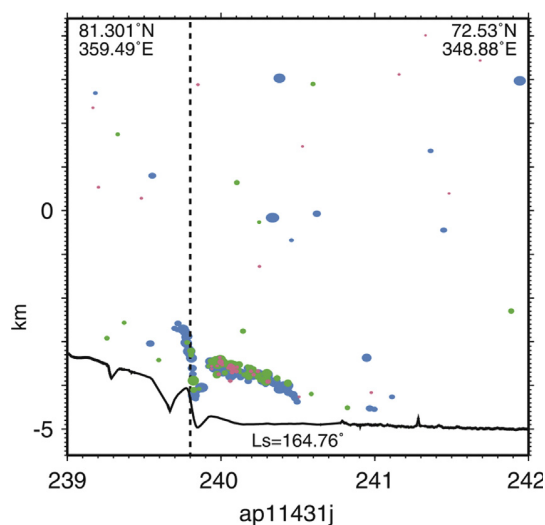


**Fig. 2.** MOLA lidar profile over edge of the north polar cap showing “nonground triggers” in colored dots above the solid black line showing the ground elevation. The dotted line is the terminator.  $L_s=164$  is northern fall and the north polar hood is responsible for the cloud returns. From [40]. (For interpretation of the references to color in this figure legend, the reader is referred to the web version of this article.)

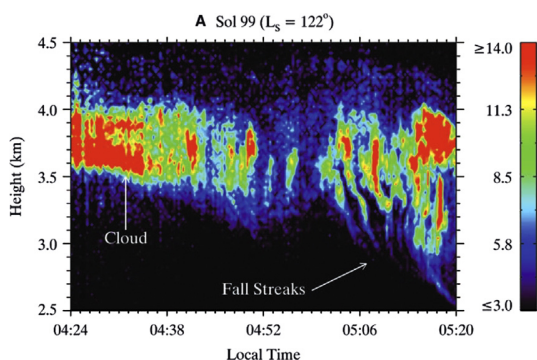


**Fig. 3.** Phoenix lidar vertical scan showing fall streaks in northern Martian summer as they pass 4 km high over the lander. From [42].

particle sizes or shapes, nor measure the H<sub>2</sub>O or CO<sub>2</sub> vapor abundances (Table 1).

The MOLA instrument did demonstrate the ability to detect optically thin Martian dust devils [40]. Consequently, one can have confidence that ASPEN will be capable of monitoring dust loading and activity, including that associated with the eruption of ‘geysers’ in the south polar ‘Cryptic’ Region [8] – because the ASPEN detectors are designed not to saturate over the relatively high albedo Martian ice caps.

## 2.2. Previous lidar mission – Phoenix

The Phoenix spacecraft landed in the Vastitas Borealis region near the northern pole of Mars (at 68.2° N) in May 2008 and operated for 5 months or 152 Martian days (one summer and fall period) [41]. The Phoenix metrology station included a vertical pointing Nd:YAG lidar operating at 1.064 and 0.532 μm. The lidar system successfully detected aerosol structures consistent with Martian cirrus clouds (see Fig. 3) and in particular the ‘virga’ or “Mare’s Tails” (ice particles falling from their formation site in the main cloud deck) as they passed over the lander during the local night [42]. Phoenix lidar data has also been used to measure the height of the Planetary Boundary Layer (around 4 km) and infer dust grain sizes (using ratios of the two channels) around 1.2–1.4 μm [43]. Having no polarization capability, the Phoenix lidar could not directly determine grain shapes. We consider the Phoenix lidar to be a useful pathfinder for more ambitious lidar systems such as ASPEN.

## 2.3. Previous lidar mission – CALIPSO

The CALIOP laser onboard the Cloud Aerosol Lidar and Infrared Pathfinder Satellite Observations (CALIPSO) spacecraft was launched in April 2006 and is still in operation. With an orbit ~700 km, it is part of the ‘A-Train’ of Earth observing satellites. The CALIOP laser operates at 1.064 and 0.532 μm, measuring linear polarization in the latter band. The instrument was designed and tested at Ball Aerospace and is operated jointly by NASA and CNES [44].

The surface footprint of the CALIOP is ~100 m and the vertical resolution is 30–60 m. Fig. 4 shows an example of

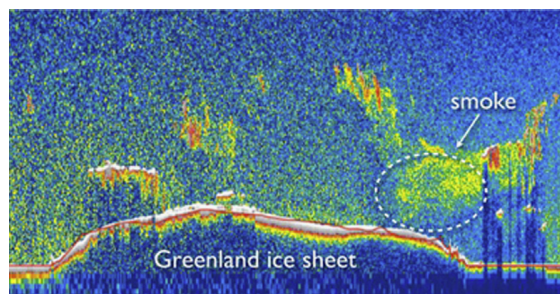


**Fig. 4.** CALIPSO satellite vertical scan over Greenland ice sheet showing aerosol soot due to wildfires. From [45].

a CALIPSO observation of soot from Arctic wildfires drifting over Greenland [45]. The sensitivity to the aerosols associated with the fires provides a clear demonstration of lidar utility for monitoring/characterizing dust and cloud activity across multiple scales, as well as for studies of low lying fogs and sublimation flow events near the Martian surface. CALIPSO has also been used to monitor the height of the terrestrial planetary boundary layer [13], a useful precursor experiment for ASPEN at Mars.

Although CALIOP does not exhibit the same wavelength flexibility and polarimetric capability (i.e. does not measure the full returned Stokes vector) of the ASPEN instrument, its enhanced abilities beyond the MOLA and Phoenix lidar provide further motivation for the ASPEN concept of an orbital lidar around Mars.

## 3. Scientific approach to achieving planned objectives

We now discuss the scientific approach to achieve the Science Objectives of the ASPEN instrument. We break the discussion below down by science theme, where each theme embodies at least four key common capabilities:

**Nadir soundings:** In common with the MOLA and Phoenix lidars, the ASPEN instrument naturally resolves the return pulse from backscattering target materials, including atmospheric constituents, gas and aerosols, clouds and multiple cloud decks and low lying fogs, in addition to the surface return.

**Composition:** The multi-wavelength nature of the instrument allows discrimination of the three major constituents of the Martian volatile cycles – CO<sub>2</sub> and H<sub>2</sub>O ice and gas, and dust.

**Grain size and distribution:** The Müller matrix polarization capability of the lidar allows determination of the scattered grain size and place limits on the size distribution.

**Seasonal changes and dynamics:** The orbital nature of the ASPEN instrument and mission profile allows us to concentrate on polar observations in order to address key scientific questions that are inaccessible to other instruments. Maps of the changes over the mission lifetime will be key to increasing our understanding and improving our interpretations of the Martian volatile cycles.

To outline the science case, we discuss below a “minimal laboratory” ASPEN instrument that could be developed to reduce engineering risks. The “minimal” nature is

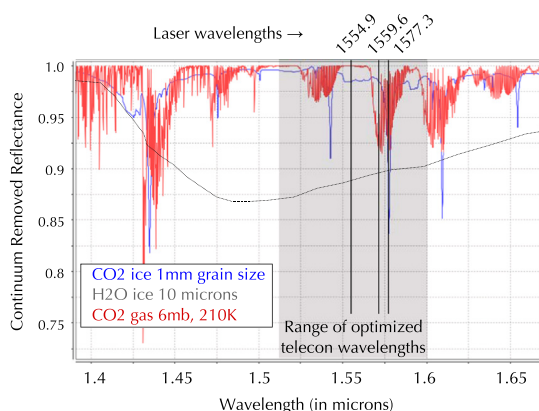


**Fig. 5.** Model reflectance spectra of CO<sub>2</sub> vapor (red, normalized to 1) CO<sub>2</sub> ice (blue) and H<sub>2</sub>O ice (gray). Both ices have been normalized to 1 at 1 μm). Black vertical lines show three laser lines to be used for the “minimal” ASPEN instrument. (For interpretation of the references to color in this figure legend, the reader is referred to the web version of this article.)

**Table 2**  
Critical bands for eventual spaceflight ASPEN detection strategy.

	CH <sub>4</sub> vapor	H <sub>2</sub> O vapor	H <sub>2</sub> O ice	CO <sub>2</sub> vapor	CO <sub>2</sub> ice
Wavelength (μm)	1.429	1.59247	1.4–1.75	1.44–1.45	1.435

captured primarily in the cost savings obtained by the use of a small number of laser wavelengths.

### 3.1. Science theme one – surface

#### 3.1.1. Detection of H<sub>2</sub>O ice and CO<sub>2</sub> ice and discrimination from vapor

In the 1.4–1.7 μm region there are several H<sub>2</sub>O and CO<sub>2</sub> ice and gas absorption bands (Fig. 5). Table 2 identifies particularly relevant bands for. Not all of these absorption bands need to be covered in a “minimal laboratory” instrument, but they may be used by an eventual spaceborne instrument.

When measured by a coarse spectrometer [46], CO<sub>2</sub> ice and vapor lines overlap and therefore can be difficult to separate [47]. However, as seen in Fig. 5, when illuminated with a narrow band laser of less than 1 nm spectral width, these bands overlap but are separable, particularly because of the nature of narrow CO<sub>2</sub> ice bands. To construct Fig. 5, we used gas band data from the HITRAN database [48] and H<sub>2</sub>O ice optical constants appropriate for 145 K [49] and CO<sub>2</sub> ice optical constants [50] to model the spectra of H<sub>2</sub>O and CO<sub>2</sub> ice with grain sizes of 10 and 1000 μm and 40% porosity [9,51], using the albedo model of Shkuratov [52].

#### 3.1.2. Simulations of the Martian polar surfaces

Several aspects of the Martian icy polar regions are not well understood. Testing and certifying the ASPEN instrument for flight will require preparation of an analog for the Martian CO<sub>2</sub> seasonal cap. This will require the marriage of the minimal laboratory instrument with a Martian test

chamber. The chamber would contain analog CO<sub>2</sub> ice slabs [53] and H<sub>2</sub>O and CO<sub>2</sub> ice particles to Martian snowpack under a 6–10 mbar CO<sub>2</sub> atmosphere. The amount of dust mixed into the ice surface is not well constrained [54]. During the course of testing this type of instrument, one would anticipate using a range of suspended and surface dust compositions, grain shapes and size distributions to simulate realistic dusty Martian snowpacks and dust-laden atmospheres.

#### 3.1.3. Ice identification using multiple wavelengths

To differentiate ice composition, we will use a ratio of the backscattered reflectance at the absorption band center to that outside the relevant absorption feature. The minimal instrument will use only 3 lasers; therefore, it will only be able to simultaneously detect three phases unambiguously. A ratio of 1.5773/1.5549 μm will give CO<sub>2</sub> ice, 1.5696/1.5549 μm will give CO<sub>2</sub> gas and 1.5549/1.5773 μm will give the slope of the H<sub>2</sub>O ice absorption feature, allowing H<sub>2</sub>O ice abundance estimates. More lines would be added in the 1.4–1.7 μm region in the eventual orbital instrument to provide simultaneous sensitivity to H<sub>2</sub>O and CO<sub>2</sub> gas and ice phases (Table 2).

#### 3.1.4. Surface pressure maps and partial pressure of H<sub>2</sub>O vapor

Using the multiple wavelength DIAL technique discussed above, the ASPEN instrument will be able to measure the atmospheric pressure using the CO<sub>2</sub> gas band, and partial pressure of H<sub>2</sub>O vapor. It will be able to discriminate these from surface ices. Given that CO<sub>2</sub> comprises more than 95% of the Martian atmosphere, ASPEN can essentially provide the atmospheric surface pressure (generally to 1%). Thus, ASPEN will be able to produce global surface total pressure and water vapor partial pressure maps for the entire mission, for each multiple wavelength nadir sounding measurement.

These seasonal maps of surface pressure will be a unique dataset that will be of great value for the Mars climate modeling community, and can be used to generate wind maps, assess atmospheric heat transfer and address questions of current global energy dynamics, including katabatic winds over the polar regions [55], on cap CO<sub>2</sub> depositional winds [56–58] (the “Houben effect”), transfer of H<sub>2</sub>O between caps and regolith [59] and countless other Martian atmospheric phenomena.

### 3.2. Science theme two – ice clouds

#### 3.2.1. CO<sub>2</sub> ice clouds and CO<sub>2</sub> ice snowfall

CO<sub>2</sub> ice clouds on Mars were first suggested by Gierasch and Goody [60] and were thought to have been observed by the Mariner 6 and 7 infrared spectrometer [61] although that observation has been disputed [62]. Low brightness temperatures measured by Viking were attributed to CO<sub>2</sub> clouds or perhaps snowfall by Forget [63]. Montmessin et al. [64] reported detection of CO<sub>2</sub> ice clouds with grain sizes of less than 100 nm at 100 km above the Martian surface using PFS/SPICAM in an occultation study. Subsequently, the CO<sub>2</sub> cloud formation process has been modeled accounting for homogenous nucleation conditions in the

CO<sub>2</sub> rich atmosphere [65], and the occurrence times have been linked to wave induced cold pockets in the Martian mesosphere, although the observed opacities suggest an external nucleation particle source (meteorites) is necessary [66].

An analysis of MCS observations [2] also indicated substantial cloudiness during the polar night, assumed to be composed of CO<sub>2</sub> ice due to the cold atmospheric temperatures. However, being a limb sounder, the MCS instrument cannot regularly access the lower 10–15 km of the vertical column of the Martian atmosphere, where the lion's share of atmospheric dust and ice reside. This limitation is the result of the physics of radiative transfer (i.e. multiple scattering effectively obscures any information from this region [67]). Models of the MCS observations suggest that the sounder dataset often misidentifies CO<sub>2</sub> clouds as H<sub>2</sub>O clouds 40% of the time [68,69].

Understanding the distribution of CO<sub>2</sub> ice clouds is important because they may have a net surface warming effect [70–72] and may initiate vigorous mixing of the polar night atmosphere, affecting the vertical distribution of temperatures, aerosols and gases [73].

MOLA was optimized for topography mapping, not cloud detection. MOLA was able to detect clouds that lay within 20 km of the surface, and it found clouds mostly on the nightside and in the winter polar hoods of the planet [37,40]. Tantalizingly, MOLA found two types of clouds based on height and structure of the return echoes [38]; however, MOLA could not (1) detect clouds at greater than 20 km altitude; (2) distinguish definitively between CO<sub>2</sub> and H<sub>2</sub>O ice; nor (3) measure albedo or detect presence of gas/dust jets over the seasonal CO<sub>2</sub> ice caps (low dynamic range caused saturation).

Nonetheless, coincident TES brightness-temperature observations and radio occultation measurements led MOLA researchers to suggest the clouds they observed in the polar hoods were most likely CO<sub>2</sub> ice clouds [38] and CO<sub>2</sub> ice precipitation [74]. MOLA also observed some mid-latitude nighttime clouds that may have been composed of H<sub>2</sub>O ice [40]. Confirmation and extension of these observations and identification of CO<sub>2</sub> or H<sub>2</sub>O clouds is critical to improving our understanding of the Martian thermal budget.

### 3.2.2. Polar hood water ice clouds

The polar caps are covered by water ice clouds during winter and these will be a major focus of the ASPEN mission.

The internal structure of clouds and precipitation streaks were observed over a limited region of the Martian north pole by the Phoenix lidar [42] in addition to near-surface fogs [75]. These lidar cloud observations indicate Martian cloud internal structure is likely quite variable and information-rich. Detection of planet-wide four-dimensional (three spatial dimensions and variations with time) cloud decks and mapping of precipitation should be possible using ASPEN.

*North–south polar hood comparison:* The Martian polar hood clouds play a role of transporting water ice from the polar caps towards the equatorial regions. The northern hemisphere of Mars is comparatively water ice rich and as a result the northern polar hood has higher optical depth than the south polar hood [76]. The north polar hood lasts

longer (75% of the Martian year, from  $L_s = 150\text{--}30^\circ$  compared to 50% of the Martian year,  $L_s = 10\text{--}70^\circ$  and  $100\text{--}200^\circ$  [77]) and encloses the entire cap, whereas the south polar hood is an annular ring [78]. Benson et al. [77] established that the south polar hood is composed of two decks, and ASPEN is well suited to investigating and contrasting the physical properties of both decks, including grain size, shapes and orientations.

Vortex clouds around the edge of the cap, including streak clouds and lee wave clouds, have been observed in the north (where they are more common) and in the south (where they are much weaker) using Viking orbiter [79] and Mars Orbiter camera images [80]. “Annular bands” of low ice and dust opacity have been detected using the TES instrument over the north pole, perhaps indicating “flushing dust storms” [81]. These annular bands have not been detected in the south polar region, perhaps because of the thermal response of the surface which may corrupt the observations. ASPEN is ideally suited to determine whether the annular bands and streak waves are related. The instrument will carry out searches for these features in both north and south polar regions with high sensitivity.

Montmessin et al. [25] modeled many of the properties of the polar hood using a Global Climate Model. They predicted the strengthening of polar hoods at the start and end of the winter season, which will be verified by ASPEN. Montmessin et al. also modeled streak or spiral waves, and found that they only developed structure in the north polar region, where the hood clouds were much stronger.

ASPEN is ideally suited to determine whether the annular bands and spiral streak waves are related. The instrument will carry out searches for these features in both north and south polar regions with high sensitivity.

### 3.2.3. Cloud nucleation and ice crystal shapes

There have been numerous attempts to model the grain shapes of CO<sub>2</sub> and H<sub>2</sub>O ice particles that would be appropriate to Mars, including experimental observations of CO<sub>2</sub> ice grains formed under Martian conditions that are octahedrons (or bipyramidal) [82], and theoretical models of CO<sub>2</sub> ice grains suggesting cubic or truncated octahedral forms [83]. Because cuboctahedra are not oriented by air resistance as they fall, CO<sub>2</sub> ice clouds on Mars may not produce sundogs but will produce halos [84].

As already discussed, ASPEN will measure the back-scattered Mueller matrix polarization and measure the linear depolarization ratio in order to shed light on the shape (in particular the asphericity) of ice cloud particles as a function of height. The multi-wavelength nature of the observations will also shed light on small (1 μm and smaller) size distributions [85], potentially shedding light on ice nucleation dynamics [86] and surface alteration processes for amorphous phases [87,88]. Thus, ASPEN will be able to address grain sizes and shapes for multiple coincident cloud decks.

## 3.3. Science theme three – dust aerosols

ASPEN is designed to be sensitive to Martian dust and aerosols. Virga (fall streaks) and precipitation mapping are key parts of our third science theme.

Suspended dust also will have an effect on the detection of ice clouds. This will be particularly true during southern summer dust events. There is evidence that most Martian dust displays a limited size range (average grain sizes of 1.3–1.8  $\mu\text{m}$  [89]) and the polarization returns of these particles will be different from very fine  $\text{CO}_2$  ice clouds [90] – although some water ice clouds may show similar characteristics. The polar regions experience lower amounts of dust than the rest of the planet [91] however the effect of dust aerosols is of critical importance. Dust storms are a repeating global phenomenon, affecting the albedo of the polar caps, with many local and regional storms originating in the polar regions and following “dust tracks” across the Martian globe [92].

### 3.3.1. Polarization measurements

The proposed instrument would be the first to obtain polarization measurements of planetary materials under Martian conditions over the 1.4–1.7  $\mu\text{m}$  region. Previous terrestrial studies have proven the utility of polarized light scattered from ice crystals in the atmosphere [93] and on snowpack surfaces [94–96]. *ASPEN* will be capable of measuring the full Stokes vector returned from the linearly/circularly polarized transmitted beam.

### 3.3.2. Discriminating dust aerosols and ice particles

The eventual space instrument will discriminate dust from ice using (1) absence of  $\text{CO}_2/\text{H}_2\text{O}$  ice absorption bands, (2) polarization returns, and (3) detection height to discriminate airborne dust. Methods have been developed for analyzing the depolarization ratio from *CALIPSO* to characterize the size distribution of airborne dust [97]. *ASPEN*'s multi-wavelength capability will enhance the effectiveness of this method.

### 3.3.3. Rationale for full Müller matrix measurements

The Stokes Vector (Stokes, 1852; van de Hulst, 1957) is used to describe an electromagnetic field  $E$ , with perpendicular and parallel amplitudes  $E_{\perp}$  and  $E_{\parallel}$  is defined as

$$\begin{aligned} I &= \langle E_{\parallel} E_{\parallel}^* \rangle + \langle E_{\perp} E_{\perp}^* \rangle \\ Q &= \langle E_{\parallel} E_{\parallel}^* \rangle - \langle E_{\perp} E_{\perp}^* \rangle \\ U &= \langle E_{\parallel} E_{\perp}^* \rangle + \langle E_{\perp} E_{\parallel}^* \rangle \\ V &= i(\langle E_{\parallel} E_{\perp}^* \rangle - \langle E_{\perp} E_{\parallel}^* \rangle) \end{aligned} \quad (1)$$

where angle brackets indicate a time average and asterisks indicate complex conjugation.

The optical effect of an atmospheric component may then be expressed using its angle-dependent, light scattering Müller matrix as follows:

$$\mathbf{I} = \mathbf{M} \cdot \mathbf{I}_0 = \begin{pmatrix} M_{11} & M_{12} & M_{13} & M_{14} \\ M_{21} & M_{22} & M_{23} & M_{24} \\ M_{31} & M_{32} & M_{33} & M_{34} \\ M_{41} & M_{42} & M_{43} & M_{44} \end{pmatrix} \begin{pmatrix} I_0 \\ Q_0 \\ U_0 \\ V_0 \end{pmatrix} \quad (2)$$

where subscript 0 means ‘incident’ and the Müller matrix of an optical system is represented by elements  $M_{11}, \dots, M_{44}$ . Normal optical remote sensing only measures element  $M_{11}$  and passive linear polarization experiments measure  $M_{11}$ ,  $M_{21}$  and  $M_{31}$ . Passive circular polarization experiments measure  $M_{41}$ . Active Müller matrix measurements, such as

the project proposed here, measure all 16 elements of the Müller matrix.

*ASPEN* will measure the backscattered depolarization (degree of linear polarization or DOLP) ratio, which will give further information on particle sizes and shapes. In terms of the returned Stokes matrix, the equation for the DOLP is

$$\text{DOLP} = \frac{\sqrt{(Q^2 + U^2)}}{I} \quad (3)$$

Spherical or near-spherical hydrometeors (e.g. ice or rain drops) do not depolarize backscattered light; whereas, hexagonal crystals and other shape do. The DPOL ratio for spherical droplets is 0 due to symmetry and typically 0.2–0.8 due to scattering from a variety of asymmetric ice particles [98]. This phenomenon is used in the analysis of *CALIPSO* cloud data to detect oriented ice plates in terrestrial clouds [99]. On Earth, lidar measurements have been used to map the internal structure of clouds where grain shapes change [100–103] and determine the height of oriented crystals and rain clouds [104]. *CALIPSO* data have also been used to map instantaneous connections between cloud vertical structure (via particle orientation) and large-scale climate [105]. This application offers exciting possibilities for the mapping of large scale Martian weather cycles with *ASPEN*.

*ASPEN* will also create maps of the backscattered degree of circular polarization (DOCP) ratio, which in terms of the returned Stokes matrix is given by

$$\text{DOCP} = \frac{V}{I} \quad (4)$$

Circular polarization has been shown to decrease with length of travel through a diffuse target (the circular polarization memory effect [106]). Circular polarization measurements are much less common in lidar instruments, but by measuring the circular depolarization of Martian clouds we anticipate to be able to measure their optical depth independently [107] of the degree of returned power, which will put tighter constraints on the inverse problems required to solve for the characteristics of the Martian atmosphere. The degree of circular polarization ratio has also been proposed to help discriminate cloud particle sphericity [108].

Fig. 6 displays 16 Müller matrix hemispherical maps for spherical targets produced using the adding-doubling approach [109]. The symmetry of these hemispherical maps [110] allows us to differentiate spherical and non-spherical and Rayleigh scattering target materials [90], and this capability is an important aspect of the *ASPEN* aerosol and cloud mapping approach.

## 3.4. Science matrix

Table 3 presents the science matrix for the *ASPEN* project. The three scientific themes of the instrument (Surface, Ice Clouds and Dust Aerosols) are linked to project science objectives. The objectives are then addressed individually by the instrument capabilities.

Fig. 7 gives a diagrammatic representation of the instrument and science themes of surface, ice clouds and dust aerosols.

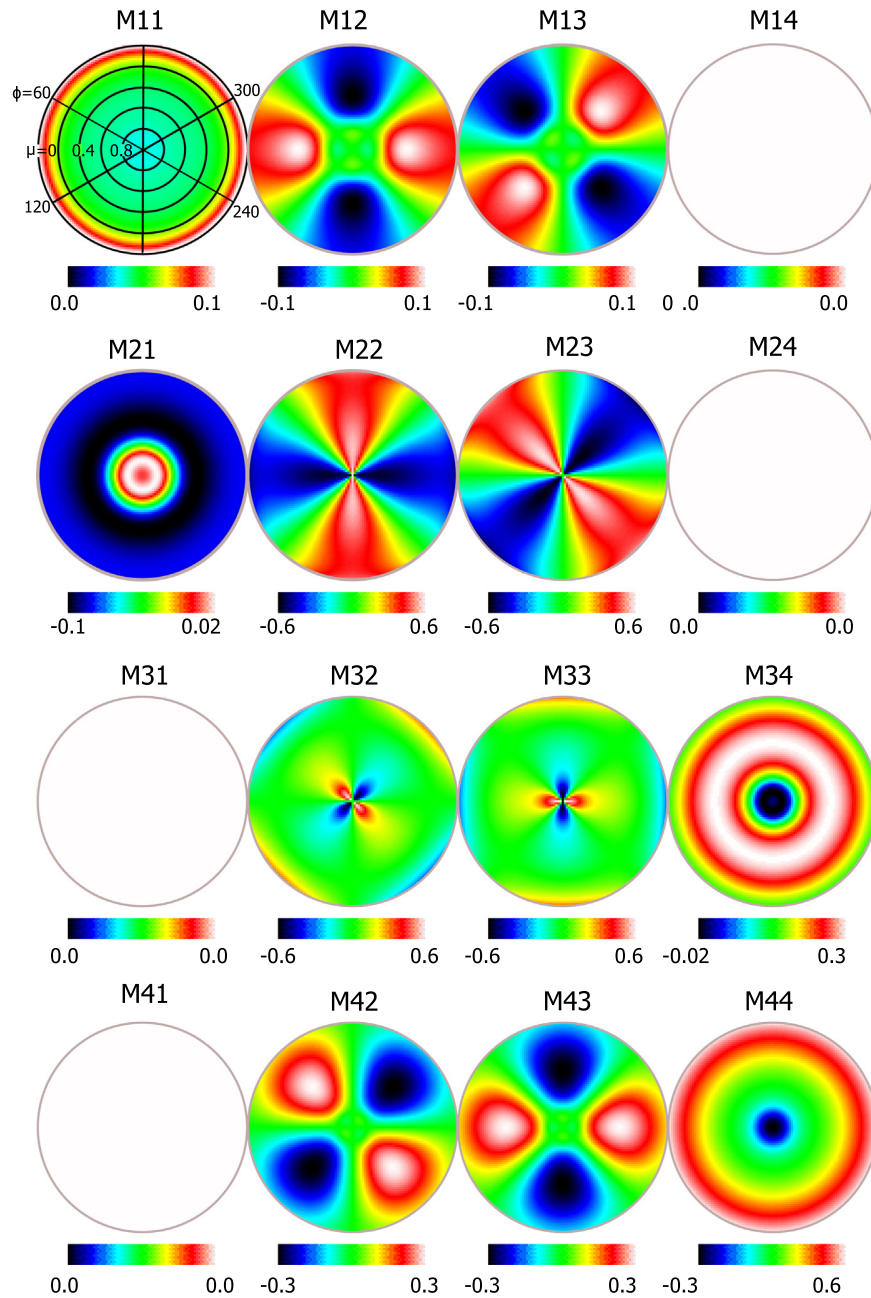


Fig. 6. Müller matrix images of backscattered photons scattered from spherical target modeled by using an adding-doubling radiative transfer model. The laser is incident normal to the target. Color scales indicate intensity relative to the  $M_{11}$  element. From [90].

#### 4. Implementation paths

##### 4.1. Technological approach and methodology

Multi-wavelength laser operations are challenging and will remain so for the foreseeable future. However, an opportunity exists to use fiber laser amplifier technology developed by the telecommunications industry to make critical measurements in a spaceflight mission.

The currently envisioned spacecraft instrument utilizes multiple diode lasers, each operable at a different wavelength, amplified by a fiber laser stage. The receiver side will consist of a telescope coupled to an indium gallium arsenide (InGaAs) multi-pixel avalanche photo detector (APD). The eventual flight instrument will be scaled to operate at ranges of 250–320 km, similar to the MRO orbit. This is around half the altitude of the  $\sim 700$  km altitude CALIPSO mission.

**Table 3**

Science matrix for the ASPEN project, linking science themes and objectives of the instrument to capabilities of the proposed instrument.

Science themes	Measurement objectives	Instrument requirement
<b>Science Theme 1. Surface.</b> To detect, map and quantify deposition of H <sub>2</sub> O and CO <sub>2</sub> ice during the polar night	1. Composition. Differentiate surface CO <sub>2</sub> ice and H <sub>2</sub> O ice	Use NIR laser DIAL technique to differentiate ices
	2. Grain shape and size. Map CO <sub>2</sub> ice and H <sub>2</sub> O ice grain size/shape properties	Use DIAL and polarization to map ice properties
	3. Seasonal changes. Map changes in height as ice is deposited	Use timed laser returns to create high res DTMs to find changes in snow pack height
	4. Seasonal changes. Determine nature of slab ice south cryptic region [4,8] and re-observe transient “halo” events [117]	Use NIR laser reflectance DIAL technique to differentiate ices and polarization to determine properties
	5. Nadir soundings. Monitor thermal cold spot activity and determine whether they are due to CO <sub>2</sub> snow, CO <sub>2</sub> clouds, blizzards or surface ice [63,74,119]	Use NIR laser reflectance DIAL technique to differentiate ices and polarization to determine properties
	6. Surface pressure. Monitor surface pressure and partial pressure of H <sub>2</sub> O and produce global, seasonal maps of surface pressure dynamics	Use NIR laser reflectance DIAL to derive total atmospheric pressure and also H <sub>2</sub> O partial pressure
<b>Science Theme 2. Ice Clouds.</b> To identify and map fogs, clouds and cloud properties inside and outside the polar hood, on a daily basis.	1. Nadir soundings. Map cloud heights up to 100 km above Martian surface, detect multiple clouds decks	Use NIR reflectance to measure albedo of cloud ice particles
	2. Composition. Determine cloud compositions and find CO <sub>2</sub> -H <sub>2</sub> O ice clusters [118]	Use NIR multiple channel DIAL reflectance technique
	3. Grain shape and size. Map cloud particle albedo, size and orientation	Use polarization to measure albedo of ice particles
	4. Nadir soundings. Discriminate fogs from H <sub>2</sub> O ice deposition on both CO <sub>2</sub> ice caps [15,16,58]	Use timed laser returns to discriminate low fogs from surface ice
<b>Science Theme 3. Dust Aerosols.</b> Map dust storms, planetary boundary layer, precipitation and aerosol loads and particle geometries and orientations on a daily basis	1. Nadir soundings. Map Planetary Boundary Layer and aerosol particle heights all mission, determine dust cloud internal structure and observe multiple decks	Use timed laser returns and strengths to map aerosols in atmosphere
	2. Grain shape and size. Map dust aerosols properties	Use NIR polarization to measure particle properties
	3. Seasonal changes. Map increased dust activity over south pole geysers	Use timed laser returns and full Stokes polarization to detect geyser dynamics and timing
	4. Nadir soundings. Map convective CO <sub>2</sub> cloud towers [21]	Use polarization to detect particle orientation/dynamics

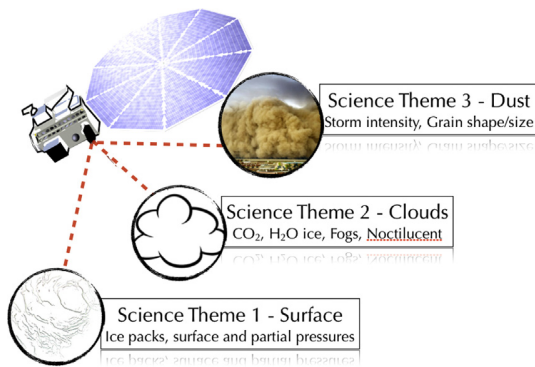


**Fig. 7.** Diagrammatic representation of ASPEN Instrument science themes.

**4.2. Radiometry analysis of spaceborne ASPEN instrument to meet science objectives**

Eq. (5) is a simplified single-scattering lidar equation [111] adequate for the evaluation of the feasibility of the proposed approach and for estimating the approximate laser pulse energy and receiver aperture size needed for

the proposed ASPEN system:

$$E(R) = E_0 \frac{\lambda}{hc} \xi B \left( \frac{A_r}{R^2} \right) T^2 \tag{5}$$

where  $E$  is in photons returned from range  $R$ , given the transmitted pulse energy  $E_0$  in Joules,  $\xi$  is the receiver efficiency factor,  $B$  is the target backscatter efficiency factor (for hard targets  $B$ =surface reflectivity ( $\text{sr}^{-1}$ ), for distributed atmospheric targets (aerosols and clouds)  $B = B_\pi(R)c \delta t/2$  where  $B_\pi$  is the volume backscatter cross section ( $\text{m}^{-1}\text{sr}^{-1}$ ),  $\Delta t$  the receiver range bin integration time, and  $c$  the speed of light),  $T$  the transmission of the atmosphere between the lidar and the target,  $A_r$  the area of the receiving telescope, and  $h$  is Planck’s constant.

The receiver efficiency factor  $\xi$  takes into account (1) the transceiver optical losses including spectral filtering and (2) the detector collection efficiency. For the first factor, a high optical efficiency with a narrowband filter for daylight ops may reach ~50% (this may be as good as 70%, but we are being conservative). For the second factor, a good photon detector will have a collection efficiency of ~30%. So, a practical efficiency factor should be  $\xi \sim 15\%$ .

The transmission factor  $T$  is the transmissivity of the atmosphere. With no dust or clouds,  $T$  would be near 1 in the thin Martian atmosphere. On Mars there is a minimal background dust opacity, so we will choose a transmission  $T \sim 0.9$  so that  $T^2 \sim 0.81$ .

Background Light at Mars. We can calculate the background light at Mars as follows:

$$E_{bg} = \left(\frac{\lambda}{hc}\right) \pi (\theta/2)^2 \delta S_c B \xi A_r \quad (6)$$

where  $\theta$  is the instrument field of view (assumed 150  $\mu$ R, see Table 1),  $\delta$  is the filter bandpass (assumed 1 nm) and  $S_c$  is the solar radiance at Mars at 1.5  $\mu$ m (based on a figure of 0.25 W/m<sup>2</sup>/nm at 1.5  $\mu$ m at the top of Earth's atmosphere, and scaled to Mars using  $S_c = 0.25 (D_{earth}/D_{mars})^2 = 0.25(150 \times 10^9 / 228 \times 10^9)^2 = 0.108$  W/m<sup>2</sup> nm). Using these values in Eq. (6), we calculate:

$$E_{bg} = \frac{1.5 \times 10^{-6}}{6.6 \times 10^{-34} \times 3 \times 10^8} \pi \left( (150 \times 10^{-6}) / 2 \right)^2 \times (1 \times 10^{-9}) (0.108) (0.08) (0.15) \pi (0.8/2)^2$$

which comes to 1.09 photons/s. When this is multiplied by a typical range bin of 200 ns, we have a background of  $2.2 \times 10^{-7}$  photons/shot/30 m range bin.

*Detector dark current:* Noise due to detector dark current is inherently produced by any cooled detector. For our NIR application, a typical figure of 200 dark current photons/second is typical, and again assuming a range bin of 200 ns, this translates to  $4 \times 10^{-5}$  photons/shot/30 m range bin.

Thus the expected background light at Mars is less than the expected detector dark current, but they are both expected to be small in comparison to expected photon collection rates for typical targets for each science theme, which we now calculate.

Science Theme 1. Surface (hard target) sensitivity: For returns from a hard target with an albedo of 0.5 (a typical Martian CO<sub>2</sub> ice NIR albedo [1]) and diffuse surface reflectivity  $\sim 0.08$  sr<sup>-1</sup> (divide albedo by  $2\pi$ sr) and receiver diameter  $\sim 0.8$  m (see Table 1), pulse energies of  $\sim 40$   $\mu$ J will produce the following calculation using Eq. (5):

$$E(R) = 4 \times \frac{10^{-5} \times 1.5 \times 10^{-6}}{6.6 \times 10^{-34} \times 3 \times 10^8} \times (0.15) \times (0.08) \frac{\pi \times (0.8/2)^2}{(2.5 \times 10^5)^2} \times 0.9^2 = 23 \text{ photons/shot}$$

Science Theme 2. High altitude clouds (Diffuse target) discrimination sensitivity: Measurements by Felton et al. [112] suggest that  $\beta_\pi$  for terrestrial polar stratospheric clouds (PSCs) are  $\sim 1-10 \times 10^{-7}$  m<sup>-1</sup> sr<sup>-1</sup>. Assuming  $\beta_\pi = 1 \times 10^{-7}$  m<sup>-1</sup> sr<sup>-1</sup> for Martian PSCs, a range to the PSC of 180 km (i.e. cloud top height of  $\sim 70-100$  km [64], a 0.8 m class receiver, and a 30 m range integration gate ( $\Delta t = 200$  ns), Eq. (5) suggests signal strengths of  $\sim 0.007$  photons/shot/30 m range and a SNR  $\sim 10$  can be achieved in 0.32 s, suggesting a spatial resolution in tenuous clouds of at least 1100 m in Martian stratospheric clouds is feasible.

Science Theme 3. Dust Aerosols and Low clouds (Diffuse target) sensitivity: Assuming returns from low altitude Martian dust aerosols and water clouds or fogs have

similar characteristics to terrestrial dust and fogs [113],  $\beta_\pi \sim 2.2 \times 10^{-3}$  m<sup>-1</sup> sr<sup>-1</sup> at 532 nm, and scaling by  $\lambda^{-1}$  for particles large compared to the wavelength,  $\beta_\pi$  at 1.5  $\mu$ m is  $\sim 7 \times 10^{-5}$  m<sup>-1</sup> sr<sup>-1</sup>. Eq. (5) suggests ground fogs or dust should produce  $\sim 0.97$  photons/shot/10 m range gate from a 250 km altitude with a 0.8 m class receiver. Positive identification of CO<sub>2</sub> or H<sub>2</sub>O ice composition over the surface can be made with an optical signal-to-noise ratio (SNR)  $\sim 10$  (i.e.  $\sim 100$  photons measured) that can be achieved in 23 ms at a 4.5 kHz pulse rate (all wavelengths can be used for cloud detection), suggesting a ground sampling resolution of 78 m in fog or dust is feasible.

### 4.3. Martian mission operations

As currently envisioned, the ASPEN instrument would operate as a line profile instrument, in a similar manner to the MOLA lidar [114]. The instrument is best suited for an MGS or MRO-type 250–320 km circular orbit but could also operate in an elliptical orbit with reduced sensitivity during apoapsis. For optimized polar measurements, orbital inclination should be between 85° and 92.8° [31]. An elliptical orbit such as that mentioned in the MSO SAG document [115] would allow lidar-occultation measurements of the atmosphere, allowing the atmosphere to be viewed 'side on', thus enabling profile measurements of CO<sub>2</sub>, H<sub>2</sub>O ice and vapor in the Martian atmosphere.

*Variable local time overflight times:* Because ASPEN is not limited to daylight observations, and because much of the Martian phenomena we wish to observe is diurnally variable, we intend to vary the local time of overflight during the mission in order to further constrain the proposed hypotheses for each phenomenon. This will be of great utility for examining cold jets activity in the Cryptic region, for example. We anticipate observations over 4 temporal overpasses during the mission for example, with 3 am/3 pm, 6 am/6 pm, 9 am/9 pm and noon/midnight observations (each for 2–3 months), although this will have to be tuned as the instrument is prepared for launch, depending on the Mars season and targeting priorities.

Because of its ability to directly detect and discriminate water ice and CO<sub>2</sub> ice clouds, the instrument would be directly applicable to four of the ten science goals of the Planetary Science Decadal (PSD) Survey Mission Concept [116] listed in Table 4. The instrument would operate in both day and nighttime conditions, with greater precision during the nighttime due to less reflected background sunlight entering the instrument. During one Martian year of operations, a full

**Table 4**  
Relevance connections with proposed Planetary Science Decadal Survey Missions.

Planetary Science Decadal Survey Polar Mission Concept Goals [106]	Relevant science theme of this project
1. Mass, density and volume of seasonal CO <sub>2</sub> ice	1. Surface
2. Accumulation/ablation rates	
10. Energy exchange during polar night	2. Clouds
8. Transport of water and dust in and out of polar regions	3. Aerosols

summer and winter would be observed at each pole. This would allow an assessment of seasonal cloud and surface volatile activity in addition to monitoring the dynamics of surface and atmospheric pressure and partial pressure of H<sub>2</sub>O vapor. This would achieve the top level goals of the instrument and would be considered a complete science mission. An extended mission of an extra year of Martian operations would allow interannual comparisons and additional coverage of the ground surface.

#### 4.4. Other planetary science missions applicable for the proposed instrument

We are emphasizing the utility of the ASPEN lidar instrument for an orbital Mars mission; however the same type of instrument would be applicable for a range of future missions. It would be ideal for missions to ice covered bodies (e.g. Europa, Enceladus, Triton, even methane ice on Kuiper Belt objects) to investigate the properties of icy surfaces in low sunlight conditions. As part of a Discovery class mission to cometary bodies the system would be ideal for probing the physical properties of a coma. The instrument could also be used in a Venus orbit to probe cloud properties and structure in NIR windows of the Venusian atmosphere.

## 5. Conclusions

We have outlined the science case for a polarization lidar for an eventual orbital mission to Mars. The combination of active, multiple-wavelength measurements with polarimetry makes this instrument concept an essential option in the future inventory of spacecraft instrumentation.

The lessons learned from such an instrument would fundamentally shift our understanding of modern day volatile transport, deposition and would also have astrobiological implications for past, present and future life on Mars.

## Acknowledgments

AJB acknowledges support from two grants (NNX11AP23G and NNX13AN21G) from the NASA Planetary Geology and Geophysics program run by Dr. Mike Kelley and two grants from the NASA Mars Data Analysis Program (NNX11AN41G and NNX13AJ73G) administered by Dr. Mitch Schulte. We would also like to thank Jeff Applegate, Rich Dissly, Sara Tucker, Jonathan Weinberg and Carl Weimer at Ball Aerospace for their invaluable efforts on this project.

## References

- [1] Brown AJ, Calvin WM, McGuire PC, Murchie SL. Compact Reconnaissance Imaging Spectrometer for Mars (CRISM) south polar mapping: first Mars year of observations. *J Geophys Res* 2010;115. <http://dx.doi.org/10.1029/2009JE003333>.
- [2] Hayne PO, Paige DA, Schofield JT, Kass DM, Kleinbathl A, Heavens NG, et al. Carbon dioxide snow clouds on Mars: south polar winter observations by the Mars Climate Sounder. *J Geophys Res* 2012;117:E08014.
- [3] Wolff MJ, Todd Clancy R, Goguen JD, Malin MC, Cantor BA. Ultraviolet dust aerosol properties as observed by MARCI. *Icarus* 2011;208:143–55.
- [4] Langevin Y, Douté S, Vincendon M, Poulet F, Bibring J-P, Gondet B, et al. No signature of clear CO<sub>2</sub> ice from the cryptic regions in Mars' south seasonal polar cap. *Nature* 2006;442:790–2.
- [5] Appere T, Schmitt B, Langevin Y, Douté S, Pommerol A, Forget F, et al. Winter and spring evolution of northern seasonal deposits on Mars from OMEGA on Mars Express. *J Geophys Res* 2011;116:E05001.
- [6] Titus TN, Kieffer HH, Christensen PR. Exposed water ice discovered near the south pole of Mars. *Science* 2003;299:1048–51.
- [7] Kieffer HH, Titus TN. TES mapping of Mars' north seasonal cap. *Icarus* 2001;154:162–80.
- [8] Kieffer HH, Christensen PR, Titus TN. CO<sub>2</sub> jets formed by sublimation beneath translucent slab ice in Mars' seasonal south polar ice cap. *Nature* 2006;442:793–6.
- [9] Brown AJ, Calvin WM, Murchie SL. Compact Reconnaissance Imaging Spectrometer for Mars (CRISM) north polar springtime recession mapping: first 3 Mars years of observations. *J Geophys Res* 2012;117:E00J20.
- [10] Brown AJ, Titus TN, Byrne S, Wolff M, Videen G, Colaprete A, et al. Atmospheric/Surface polarization experiment at nighttime (ASPEN). Maryland: NASA Goddard Space Flight Center; 2012 (Abstract #1110).
- [11] Jaquin F, Gierasch P, Kahn R. The vertical structure of limb hazes in the Martian atmosphere. *Icarus* 1986;68:442–61.
- [12] Petrosyan A, Galperin B, Larsen SE, Lewis SR, Määttäen A, Read PL, et al. The Martian atmospheric boundary layer. *Rev Geophys* 2011;49:RG3005.
- [13] Liu J, Huang J, Chen B, Zhou T, Yan H, Jin H, et al. Comparisons of PBL heights derived from CALIPSO and ECMWF reanalysis data over China. *J Quant Spectrosc Radiat Transf* 2014;. <http://dx.doi.org/10.1016/j.jqsrt.2014.10.011>, in press.
- [14] Langevin Y, Bibring J-P, Montmessin F, Forget F, Vincendon M, Douté S, et al. Observations of the south seasonal cap of Mars during recession in 2004–2006 by the OMEGA visible/near-infrared imaging spectrometer on board Mars Express. *J Geophys Res* 2007;112. <http://dx.doi.org/10.1029/2006JE002841>.
- [15] Inada A, Richardson MI, McConnochie TH, Strausberg MJ, Wang H, Bell II JF. High-resolution atmospheric observations by the Mars Odyssey Thermal Emission Imaging System. *Icarus* 2007;192:378–95.
- [16] Titus TN. Thermal infrared and visual observations of a water ice lag in the Mars southern summer. *Geophys Res Lett* 2005;32. <http://dx.doi.org/10.1029/2005GL024211>.
- [17] Forget F, Pollack JB. Thermal infrared observations of the condensing Martian polar caps: CO<sub>2</sub> ice temperatures and radiative budget. *J Geophys Res-Planets* 1996;101:16865–79.
- [18] Hayne PO, Paige DA, Heavens NG. The role of snowfall in forming the seasonal ice caps of Mars: models and constraints from the Mars climate Sounder. *Icarus* 2013;231:122–30.
- [19] Weiss BP, Ingersoll AP. Cold spots in the Martian polar regions: evidence of carbon dioxide depletion? *Icarus* 2000;144:432–5.
- [20] Piqueux S, Christensen PR. North and south subice gas flow and venting of the seasonal caps of Mars: a major geomorphological agent. *J Geophys Res* 2008;113. <http://dx.doi.org/10.1029/2007JE003009>.
- [21] Colaprete A, Haberle RM, Toon OB. Formation of convective carbon dioxide clouds near the south pole of Mars. *J Geophys Res* 2003;108. <http://dx.doi.org/10.1029/2003JE002053>.
- [22] Ma Y, Gong W, Wang P, Hu X. New dust aerosol identification method for spaceborne lidar measurements. *J Quant Spectrosc Radiat Transf* 2010;112:338–45.
- [23] Lu X, Jiang Y, Zhang X, Wang X, Spinelli N. Two-wavelength lidar inversion algorithm for determination of aerosol extinction-to-backscatter ratio and its application to CALIPSO lidar measurements. *J Quant Spectrosc Radiat Transf* 2010;112:320–8.
- [24] Colaprete A, Toon OB. The radiative effects of Martian water ice clouds on the local atmospheric temperature profile. *Icarus* 2000;145:524–32.
- [25] Montmessin F, Forget F, Rannou P, Cabane M, Haberle RM. Origin and role of water ice clouds in the Martian water cycle as inferred from a general circulation model. *J Geophys Res* 2004;109. <http://dx.doi.org/10.1029/2004JE002284>.
- [26] Michaels TI, Colaprete A, Rafkin SCR. Significant vertical water transport by mountain-induced circulations on Mars. *Geophys Res Lett* 2006;33:L16201. <http://dx.doi.org/10.1029/2006GL026562>.
- [27] Rafkin SCR. The potential importance of non-local, deep transport on the energetics, momentum, chemistry, and aerosol distributions in the atmospheres of Earth, Mars and Titan. *Planet Space Sci* 2011;60:147–54.

- [28] Osterloo MM, Hamilton VE, Bandfield JL, Glotch TD, Baldrige AM, Christensen PR, et al. Chloride-bearing materials in the southern highlands of Mars. *Science* 2008;319:1651–4.
- [29] Sparks W, Hough JH, Germer TA, Robb F, Kolokolova L. Remote sensing of chiral signatures on Mars. *Planet Space Sci* 2012;72:111–5.
- [30] NASA. Solar System exploration – 2006 solar system exploration roadmap. NASA; 2006.
- [31] Calvin W, Allen M, Banerdt WB, Banfield D, Campbell BA, Christensen PR, et al. Report from the 2013 Mars Science Orbiter (MSO) Second Science Analysis Group. Pasadena, CA: JPL; 2007.
- [32] Titus TN, Michaels TI. Determining priorities for future Mars polar research. *Eos Trans AGU* 2009;90:351.
- [33] Titus TN, Prettyman TH, Brown AJ, Michaels TI, Colaprete A. Mars ice condensation and density orbiter. Houston, TX: LPI; 2010.
- [34] Wulfmeyer V, Walther C. Future performance of ground-based and airborne water-vapor differential absorption lidar. I. Overview and theory. *Appl Opt* 2001;40:5304–20. <http://dx.doi.org/10.1364/AO.40.005304>.
- [35] Machol JL, Ayers T, Schwenz KT, Koenig KW, Hardesty RM, Senff CJ, et al. Preliminary measurements with an automated compact differential absorption lidar for the profiling of water vapor. *Appl Opt* 2004;43:3110–21. <http://dx.doi.org/10.1364/AO.43.003110>.
- [36] Smith DE, Zuber MT, Solomon SC, Phillips RJ, Head JW, Garvin JB, et al. The global topography of Mars and implications for surface evolution. *Science* 1999;284:1495–503.
- [37] Pettengill GH, Ford PG. Winter clouds over the north Martian polar cap. *Geophys Res Lett* 2000;27:609–12.
- [38] Ivanov AB, Muhleman DO. Cloud Reflection observations: results from the Mars Orbiter Laser Altimeter. *Icarus* 2001;154:190–206.
- [39] Hu R, Cahoy K, Zuber MT. Mars atmospheric CO<sub>2</sub> condensation above the north and south poles as revealed by radio occultation, climate sounder, and laser ranging observations. *J Geophys Res* 2013;117:E07002.
- [40] Neumann GA, Smith DE, Zuber MT. Two Mars years of clouds detected by the Mars Orbiter Laser Altimeter. *J Geophys Res* 2003;108.
- [41] Smith PH, Tamppari LK, Arvidson RE, Bass D, Blaney D, Boynton WV, et al. H<sub>2</sub>O at the Phoenix landing site. *Science* 2009;325:58–61.
- [42] Whiteway JA, Komguem L, Dickinson C, Cook C, Illnicki M, Seabrook J, et al. Mars water-ice clouds and precipitation. *Science* 2009;325:68–70. <http://dx.doi.org/10.1126/science.1172344>.
- [43] Komguem L, Whiteway JA, Dickinson C, Daly M, Lemmon MT. Phoenix LIDAR measurements of Mars atmospheric dust. *Icarus* 2013;223:649–53.
- [44] Weimer CA, Ruppert L, Spelman J. Commissioning of the CALIPSO payload, vol. 6555. San Diego, CA: SPIE; 2007.
- [45] Box J, Tedesco M, Fettweis X, Hall D, Steffen K, Stroeve J. Greenland ice sheet albedo feedback: mass balance implications, San Francisco, CA: 2012.
- [46] Brown AJ, Sutter B, Dunagan S. The MARTE imaging spectrometer experiment: design and analysis. *Astrobiology* 2008;8:1001–11. <http://dx.doi.org/10.1089/ast.2007.0142>.
- [47] Brown AJ. Spectral curve fitting for automatic hyperspectral data analysis. *IEEE Trans Geosci Remote Sens* 2006;44:1601–8. <http://dx.doi.org/10.1109/TGRS.2006.870435>.
- [48] Rothman LS, Jacquemart D, Barbe A, Chris Benner D, Birk M, Brown LR, et al. The HITRAN 2004 molecular spectroscopic database. *J Quant Spectrosc Radiat Transf* 2005;96:139–204.
- [49] Grundy WM, Schmitt B. The temperature dependent near-infrared absorption spectrum of hexagonal H<sub>2</sub>O ice. *J Geophys Res* 1998;103:25809–22.
- [50] Hansen GB. The infrared absorption spectrum of carbon dioxide ice from 1.8 to 333mm. *J Geophys Res* 1997;102:21569–87.
- [51] Brown AJ, Byrne S, Tornabene LL, Roush T. Louth Crater: evolution of a layered water ice mound. *Icarus* 2008;196:433–45.
- [52] Shkuratov Y, Starukhina L, Hoffmann H, Arnold G. A model of spectral albedo of particulate surfaces: implications for optical properties of the Moon. *Icarus* 1999;137:235–46.
- [53] Portyankina G, Pommerol A, Aye K-M, Hansen CJ, Thomas N. Polygonal cracks in the seasonal semi-translucent CO<sub>2</sub> ice layer in Martian polar areas. *J Geophys Res* 2012;117:E02006.
- [54] Kieffer H. H<sub>2</sub>O grain size and the amount of dust in Mars' residual north polar cap. *J Geophys Res* 1990;95:1481–93.
- [55] Spiga A. Elements of comparison between Martian and terrestrial mesoscale meteorological phenomena: Katabatic winds and boundary layer convection. *Planet Space Sci* 2010;59:915–22.
- [56] Burk SD. Diurnal winds near the Martian polar caps. *J Atmos Sci* 1976;33:923–39.
- [57] Siili T, Haberle RM, Murphy JR. Sensitivity of Martian Southern polar cap edge winds and surface stresses to dust optical thickness and to the large-scale sublimation flow. *Adv Space Res* 1997;19:1241–4. [http://dx.doi.org/10.1016/S0273-1177\(97\)00276-7](http://dx.doi.org/10.1016/S0273-1177(97)00276-7).
- [58] Houben H, Haberle RM, Young RE, Zent AP. Modeling the Martian seasonal water cycle. *J Geophys Res Planets* 1997;102:9069–83.
- [59] Haberle RM, Jakosky BM. Sublimation and transport of water from the north residual polar cap on Mars. *J Geophys Res* 1990;95:1423–37.
- [60] Gierasch PJ, Goody RM. A study of the thermal and dynamical state of the Mars atmosphere. *Planet Space Sci* 1968;16:615–46.
- [61] Herr K, Pimental G. Infrared absorptions near three microns recorded over the polar cap of Mars. *Science* 1970;167:47–9.
- [62] Lopez-Valverde MA, Lopez-Puertas M, Lopez-Moreno JJ, Formisano V, Grassi D, Maturilli A, et al. Analysis of CO<sub>2</sub> non-LTE emissions at in the Martian atmosphere as observed by PFS/Mars Express and SWS/ISO. *Planet Space Sci* 2005;53:1079–87.
- [63] Forget F, Hansen GB, Pollack JB. Low brightness temperatures of Martian Polar Caps – CO<sub>2</sub> clouds or low surface emissivity. *J Geophys Res Planets* 1995;100:21219–34.
- [64] Montmessin F, Bertaux J-L, QuÉmerais E, Korabiev O, Rannou P, Forget F, et al. Subvisible CO<sub>2</sub> ice clouds detected in the mesosphere of Mars. *Icarus* 2006;183:403–10.
- [65] Listowski C, Määttänen A, Riipinen I, Montmessin F, Lefèvre F. Near-pure vapor condensation in the Martian atmosphere: CO<sub>2</sub> ice crystal growth. *J Geophys Res Planets* 2013;118:2153–71.
- [66] Listowski C, Määttänen A, Montmessin F, Spiga A, Lefèvre F. Modeling the microphysics of CO<sub>2</sub> ice clouds within wave-induced cold pockets in the Martian mesosphere. *Icarus* 2014;237:239–61. <http://dx.doi.org/10.1016/j.icarus.2014.04.022>.
- [67] Kleinböhl A, Schofield JT, Kass DM, Abdou WA, Backus CR, Sen B, et al. Mars Climate Sounder limb profile retrieval of atmospheric temperature, pressure, and dust and water ice opacity. *J Geophys Res Planets* 2009;114:E10006. <http://dx.doi.org/10.1029/2009JE003358>.
- [68] Sefton-Nash E, Teanby NA, Montabone L, Irwin PGJ, Hurley J, Calcutt SB. Climatology and first-order composition estimates of mesospheric clouds from Mars Climate Sounder limb spectra. *Icarus* 2013;222:342–56.
- [69] Hurley J, Teanby NA, Irwin PGJ, Calcutt SB, Sefton-Nash E. Differentiability and retrievability of CO<sub>2</sub> and H<sub>2</sub>O clouds on Mars from MRO/MCS measurements: a radiative-transfer study. *Planet Space Sci* 2014;97:65–84. <http://dx.doi.org/10.1016/j.pss.2014.03.015>.
- [70] Forget F, Pierrehumbert RT. Warming early Mars with carbon dioxide clouds that scatter infrared radiation. *Science* 1997;278:1273–6.
- [71] Pierrehumbert RT, Erlick C. On the scattering greenhouse effect of CO<sub>2</sub> ice clouds. *J Atmos Sci* 1998;55:1897–903.
- [72] Mischna MA, Kasting JF, Pavlov A, Freedman R. Influence of carbon dioxide clouds on early Martian climate. *Icarus* 2000;145:546–54.
- [73] Colaprete A, Barnes JR, Haberle RM, Montmessin F. CO<sub>2</sub> clouds, CAPE and convection on Mars: observations and general circulation modeling. *Planet Space Sci* 2008;56:150–80.
- [74] Titus TN, Kieffer HH, Mullins KF, Christensen PR. TES premapping data: slab ice and snow flurries in the Martian north polar night. *J Geophys Res Planets* 2001;106:23181–96.
- [75] Moores JE, Lê Komguem, Whiteway JA, Lemmon MT, Dickinson C, Daerden F. Observations of near-surface fog at the Phoenix Mars landing site. *Geophys Res Lett* 2011;38:L04203.
- [76] Smith MD. Spacecraft observations of the Martian atmosphere. *Annu Rev Earth Planet Sci* 2008;36:191–219.
- [77] Benson JL, Kass DM, Kleinb\widehathl A, McCleese DJ, Schofield JT, Taylor FW. Mars' south polar hood as observed by the Mars Climate Sounder. *J Geophys Res* 2010;115:E12015.
- [78] Benson JL, Kass DM, Kleinb\widehathl A. Mars' north polar hood as observed by the Mars Climate Sounder. *J Geophys Res* 2011;116:E03008.
- [79] Kahn R. The spatial and seasonal distribution of Martian clouds and some meteorological implications. *J Geophys Res* 1984;89:6671–88.
- [80] Wang H, Ingersoll AP. Martian clouds observed by Mars global surveyor Mars Orbiter camera. *J Geophys Res Planets* 2002;107:5078. <http://dx.doi.org/10.1029/2001JE001815>.
- [81] Horne D, Smith MD. Mars Global Surveyor Thermal Emission Spectrometer (TES) observations of variations in atmospheric dust optical depth over cold surfaces. *Icarus* 2009;200:118–28.
- [82] Foster JL, Chang ATC, Hall DK, Wergin WP, Erbe EF, Barton J. Carbon dioxide crystals: an examination of their size, shape, and scattering properties at 37 GHz and comparisons with water ice (snow) measurements. *J Geophys Res* 1998;103:25839–50.

- [83] Wood SE. Theoretical predictions of ice crystal shape in CO<sub>2</sub> clouds on Mars. American Astronomical Society; 2001.
- [84] Doherty P, Bennett C. Carbon dioxide ice halos on Mars: prediction from crystal growth experiments. Honolulu, HI: American Meteorological Society; 1986.
- [85] Brown AJ. Spectral bluing induced by small particles under the Mie and Rayleigh regimes. *Icarus* 2014;239:85–95. <http://dx.doi.org/10.1016/j.icarus.2014.05.042>.
- [86] Wood SE. Nucleation and growth of CO<sub>2</sub> ice crystals in the Martian atmosphere [Ph.D.] UCLA, 1998.
- [87] Rampe EB, Kraft MD, Sharp TG. Deriving chemical trends from thermal infrared spectra of weathered basalt: implications for remotely determining chemical trends on Mars. *Icarus* 2013.
- [88] Horgan BH, Bell JF III, Noe Dobra EA, Cloutis EA, Bailey DT, Craig MA, et al. Distribution of hydrated minerals in the north polar region of Mars. *J Geophys Res* 2014;119:114.
- [89] Wolff MJ, Smith MD, Clancy RT, Spanovich N, Whitney BA, Lemmon MT, et al. Constraints on dust aerosols from the Mars Exploration Rovers using MGS overflights and Mini-TES. *J Geophys Res* 2006;111. <http://dx.doi.org/10.1029/2006JE002786>.
- [90] Brown AJ, Xie Y. Symmetry relations revealed in Mueller matrix hemispherical maps. *J Quant Spectrosc Radiat Transf* 2012;113:644–51.
- [91] Brown AJ, Wolff MJ. Atmospheric modeling of the Martian polar regions: one mars year of CRISM EPF observations of the South Pole. Houston, TX: LPI; 2009.
- [92] Cantor BA, James PB, Calvin WM. MARCI and MOC observations of the atmosphere and surface cap in the north polar region of Mars. *Icarus* 2011;208:61–81.
- [93] Mishchenko MI, Travis LD. Satellite retrieval of aerosol properties over the ocean using polarization as well as intensity of reflected sunlight. *J Geophys Res* 1997;102:16,989–7,013.
- [94] Pal SR, Carswell AL. Multiple scattering in atmospheric clouds: lidar observations. *Appl Opt* 1976;15:1990–5.
- [95] Leroux C, Lenoble J, Brogniez G, Hovenier JW, De Haan JF. A model for the bidirectional polarized reflectance of snow. *J Quant Spectrosc Radiat Transf* 1999;61:273–85.
- [96] Sun Z, Zhao Y. The effects of grain size on bidirectional polarized reflectance factor measurements of snow. *J Quant Spectrosc Radiat Transf* 2011;114:2372–82.
- [97] Sun W, Liu Z, Videen G, Fu Q, Muinonen K, Winker DM, et al. For the depolarization of linearly polarized light by smoke particles. *J Quant Spectrosc Radiat Transf* 2012;122:233–7.
- [98] Sassen K. The polarization lidar technique for cloud research: a review and current assessment. *Bull Am Meteorol Soc* 1991;72:1848–66.
- [99] Hu Y, Winker D, Vaughan M, Lin B, Omar A, Trepte C, et al. CALIPSO/CALIOP cloud phase discrimination algorithm. *J Atmos Ocean Technol* 2009;26:2293–309. <http://dx.doi.org/10.1175/2009JTECHA1280.1>.
- [100] Toon OB, Browell EV, Kinne S, Jordan J. An analysis of lidar observations of polar stratospheric clouds. *Geophys Res Lett* 1990;17:393–6.
- [101] Mishchenko MI, Hovenier JW. Depolarization of light backscattered by randomly oriented nonspherical particles. *Opt Lett* 1995;20:1356–8.
- [102] You Y, Kattawar GW, Yang P, Hu YX, Baum BA. Sensitivity of depolarized lidar signals to cloud and aerosol particle properties. *J Quant Spectrosc Radiat Transf* 2006;100:470–82.
- [103] Chaikovskaya LI. Remote sensing of clouds using linearly and circularly polarized laser beams: techniques to compute signal polarization. In: Kokhanovsky AA, editor. *Light scattering reviews*, Part 3. Springer; 2008. p. 191–228.
- [104] Hayman M, Spuler S, Morley B. Polarization lidar observations of backscatter phase matrices from oriented ice crystals and rain. *Opt Express* 2014;22:16976–90. <http://dx.doi.org/10.1364/OE.22.016976>.
- [105] Li Y, Thompson DWJ, Stephens GL, Bony S. A global survey of the instantaneous linkages between cloud vertical structure and large-scale climate. *J Geophys Res Atmos* 2014;119(7):3770–92. <http://dx.doi.org/10.1002/2013JD020669>.
- [106] MacKintosh FC, Zhu JX, Pine DJ, Weitz DA. Polarization memory of multiply scattered light. *Phys Rev B* 1989;40:9342.
- [107] Xu M, Alfano RR. Circular polarization memory of light. *Phys Rev E* 2005;72:065601.
- [108] Hu Y-X, Yang P, Lin B, Gibson G, Hostetler C. Discriminating between spherical and non-spherical scatterers with lidar using circular polarization: a theoretical study. *J Quant Spectrosc Radiat Transf* 2003;79–80:757–64. [http://dx.doi.org/10.1016/S0022-4073\(02\)00320-5](http://dx.doi.org/10.1016/S0022-4073(02)00320-5).
- [109] De Haan JF, Bosma PB, Hovenier JW. The adding method for multiple scattering calculations of polarized light. *Astron Astrophys* 1987;183:371–91.
- [110] Brown AJ. Equivalence relations for Mueller matrix symmetries of laboratory, LIDAR and planetary scattering geometries. *J Opt Soc Am A* 2014.
- [111] Measures RM. *Laser remote sensing: fundamentals and applications*. New York: Wiley; 1984.
- [112] Felton MA, Kovacs TA, Omar AH, Hostetler CA. Classification of polar stratospheric clouds using LIDAR measurements from the SAGE III ozone loss and validation experiment. Army Research Lab Publication; 2007.
- [113] Grund CJ, Eloranta EW. The 27–28 October, 1986 fire IFO cirrus case study: cloud optical properties determined by the high spectral resolution lidar. *Mon Weather Rev* 1990;118:2344–55.
- [114] Smith DE, Zuber MT, Frey HV, Garvin JB, Head JW, Muhleman DO, et al. Mars Orbiter Laser Altimeter: experiment summary after the first year of global mapping of Mars. *J Geophys Res Planets* 2001;106:23689–722.
- [115] Farmer CB, Calvin W, Campbell B, Fox J, Haberle R, Kasting JF, et al. Mars Science Orbiter (MSO): report of the science analysis group. JPL 2006.
- [116] Calvin W, Shotwell R, Whetsel C, Pratt L, Arvidson R, Zurek R, et al. Planetary science decadal survey Mars polar climate concepts. NASA 2010.
- [117] Becerra P, Byrne S, Brown AJ. Transient bright halos on the south polar residual cap of Mars: implications for mass-balance. *Icarus* 2014;. <http://dx.doi.org/10.1016/j.icarus.2014.04.050>, in press.
- [118] Ortega IK, Määttänen A, Kurtén T, Vehkamäki H. Carbon dioxide-water clusters in the atmosphere of Mars. *Comput Theor Chem* 2011;965:353–8.
- [119] Cornwall C, Titus TN. Spatial and temporal distributions of Martian north polar cold spots before, during, and after the global dust storm of 2001. *J Geophys Res* 2009;114. <http://dx.doi.org/10.1029/2008JE003243>.